Title: Investigation of laser-induced plasma evolution in flexible pad laser shock forming with high speed camera

Author: Balasubramanian Nagarajan Zhongke Wang Sylvie Castagne H.Y. Zheng

PII: S0169-4332(14)00913-1
DOI: http://dx.doi.org/doi:10.1016/j.apsusc.2014.04.139
Reference: APSUSC 27739

To appear in: *APSUSC*

Received date: 5-11-2013
Revised date: 21-3-2014
Accepted date: 18-4-2014

Please cite this article as: B. Nagarajan, Z. Wang, S. Castagne, H.Y. Zheng, Investigation of laser-induced plasma evolution in flexible pad laser shock forming with high speed camera, *Applied Surface Science* (2014), http://dx.doi.org/10.1016/j.apsusc.2014.04.139

Highlights

- Characterization of laser-induced plasma upon laser irradiation of metal foils using high-speed camera.
- The plasma evolution characteristic in flexible pad laser shock forming (FPLSF), a sheet metal microforming process is investigated.
- The relationship between laser-induced plasma and the plastic deformation of metal foils is analyzed.
- Plasma evolution against different process variables such as laser fluence, confinement layer material and its thickness is examined.

Investigation of laser-induced plasma evolution in flexible pad laser shock forming with high speed camera

Balasubramanian Nagarajan[a,b], Zhongke Wang[a,c], Sylvie Castagne[a,b,*], H.Y. Zheng[a,c]

[a] SIMTech-NTU Joint Laboratory (Precision Machining), Nanyang Technological University, 50 Nanyang Avenue, Singapore 639798

[b] School of Mechanical and Aerospace Engineering, Nanyang Technological University, 50 Nanyang Avenue, Singapore 639798

[c] Machining Technology Group, Singapore Institute of Manufacturing Technology, 71 Nanyang Drive, Singapore 638075

* Corresponding author:

Telephone : (65) 6790 4331

Fax : (65) 6792 4062

E-mail address : scastagne@ntu.edu.sg

Postal address : School of Mechanical and Aerospace Engineering, Nanyang Technological University, 50 Nanyang Avenue, Singapore 639798

Abstract

This study investigated the effect of plasma evolution, which dominates the forming load, on the fabrication of microcraters in flexible pad laser shock forming (FPLSF) using a high speed camera. It has been found that the plasma lifetime starting from plasma formation, expansion, decaying to vanishing was less than 13.3 μs at single pulse ablation, 350 times longer than the pulse duration. When 45 pulses were applied as 5 cycles with 9 pulse train in each, the plasma size increased gradually to its maximum at the fifth or sixth pulse. There was no interference between the plasma generated from each pulse. The first pulse was sufficient for the fabrication of a crater. The crater depth and diameter increased only by 10% and 25% respectively at ablation with 45 pulses. At 45 pulses ablation for fluence from 7.3 J/cm^2 to 20.9 J/cm^2 in water confinement, the change factor appeared in descending sequence from laser fluence, maximum plasma diameter, maximum plasma pressure, to crater depth by the order of 2.86, 2.18, 1.69 and 1.47 respectively. In glass, the plasma diameter increased by 3.28 times at increasing laser fluence. The confined plasma in glass resulted in deeper craters. The smaller craters in water were attributed to the forming load diminution due to the plasma expansion, shockwave attenuation in ablative overlay, and the laser energy reduction.

Keywords

Laser-induced plasma, shock loading, laser shockwave, metal foils, microforming, confinement layer

1. Introduction

Flexible pad laser shock forming (FPLSF) is a microfabrication technique used to create microfeatures on metallic foils that can be applicable in producing various microcomponents for electronics, optics, and biomedical devices [1]. It is a sheet metal forming process using laser-induced shock pressure as the deformation force and a flexible pad as a support. Hemispherical microcraters of radius of about 500 μm and depth ranging from 80 μm to 200 μm were formed on 25 μm thick copper foils. In FPLSF, the deformation geometry is influenced predominantly by the laser-induced shock pressure which depends upon various process parameters including laser fluence, number of pulses, ablative overlay, flexible pad, confinement medium, and confinement thickness. The significant mechanism behind the induced shock pressure is the formation and propagation of plasma upon laser irradiation. The laser-induced plasma largely affects the magnitude and duration of shockwaves and hence the plastic deformation of metal foil.

A comparison of crater shapes between water and glass confinements in FPLSF revealed a significant difference in shapes at higher laser fluences; hemi-spherical craters were produced on copper foils with water confinement whereas shockwave structures were formed on copper with glass confinement [2]. This behavior was attributed to the difference in plasma and shockwave propagation between different confinement layers. However, further analysis of plasma characteristics is required to understand the effect of the confinement layer on the deformation crater shapes.

The effect of confinement layer thickness on the plastic deformation of metal foil is found to be influenced by the plasma characteristics [2-4]. When the shockwave emanating from the irradiation zone reaches the top surface of the water confinement, the water will be detached from the target surface and hence there will be no confinement of plasma [3]. This effect will cause a reduction in plasma pressure if the shockwave reaches top water surface before the arrival of peak laser pulse. Therefore, the confinement of plasma depends upon the confinement thickness and the shockwave velocity. Ocana et al. [4] found using numerical simulation that the plasma pressure increases with the increase in confinement

thickness. However, the effect of confinement thickness on the plasma behavior is yet to be examined experimentally.

Therefore, to understand the process mechanisms involved in FPLSF, it is necessary to study the formation and expansion of plasma with respect to different process parameters such as laser fluence, confinement medium, and confinement layer thickness.

Characterization of plasma has been performed extensively both quantitatively and qualitatively. Visual observation of plasma/plume in laser-material interaction has been achieved by different methods such as dye laser resonance absorption photography [5, 6], shadowgraphy [7, 8], speckle photography [9], frame and streak photography [10], and high-speed photography [11-13]. Typical characterization parameters include plasma plume size, plume edge position, plume velocity, and the plasma lifetime [13, 14]. Franco et al. [15] used streak photography technique to study the spatial and temporal evolution of laser-induced plasma by measuring the plasma absorption, initiation time, lifetime, and axial column length of the plasma. Fast photography by an ICCD camera was used to analyze the change in length and diameter of the plume core and plume periphery regions with time at different laser fluences [16]. Seto et al. [11] used two ultrahigh speed cameras (1125fps) to analyze the plasma shape and the keyhole formation in laser welding. High-speed photography is found to be an effective method to visualize and characterize the plasma to study its evolution with time [11, 12]. In most of these analyses, the geometry of the plasma was characterized to understand the plasma evolution.

In this work, the evolution of plasma with time was studied using a high-speed camera. The plasma evolution was characterized by measuring the plasma size using the plasma images acquired by the high speed camera. A comparison between the plasma size and the depth and diameter of the craters formed by FPLSF has been performed to study the effect of laser-induced plasma on the plastic deformation of metal foils. The influence of different process parameters such as laser fluence, confinement layer medium and its thickness on the plasma propagation has been analysed in detail.

2. Experimental method

2.1. FPLSF setup

The schematic illustration of FPLSF along with the plasma visualization setup using a high speed camera is shown in Fig. 1. In FPLSF, the metal foil is placed over a flexible pad which has hyperelastic material properties. A sacrificial material, the ablative overlay, is placed on top of the metal foil and exposed to high energy laser irradiation. The ablative overlay is covered with a confinement layer that is transparent to the laser beam. The laser beam passes through the confinement, vaporizes the ablative overlay and generates plasma instantaneously. The formed plasma expands as it absorbs more laser energy. As the plasma expansion is confined by the confinement layer, it creates a shockwave towards the metal foil which induces plastic deformation in foil if the shockwave pressure exceeds the dynamic yield strength of the metal. The flexible pad experiences large elastic deformation along with the plastic deformation of metal foil and retracts to its original position upon the removal of copper foil.

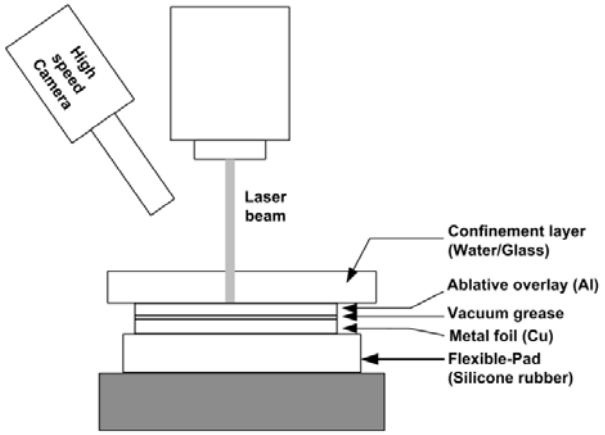

Fig. 1. Schematic of flexible pad laser shock forming with high speed camera for plasma visualization

FPLSF experiments were conducted using high power pulsed Nd:YAG laser with the following specifications: pulse width – 38 ns, wavelength – 1.064 μm, maximum pulse energy – 75 mJ at 6 KHz frequency. The laser beam was square-shaped (0.6 mm side) with flat-top intensity profile. Single laser pulse and 45 pulses were used in the experiments. Laser fluence ranging between 7.3 J/cm^2 and 20.9 J/cm^2 were used for the irradiation. Copper foil with 25 μm thickness was used as the workpiece. The copper foil was placed over a silicone rubber sheet (900 μm thick) which was used as the flexible pad. Aluminum foil with thickness of 15 μm acted as the ablative overlay on which the laser irradiation was applied. A thin layer of vacuum grease

ensured tight sealing between the copper foil and the aluminum foil. Either fused silica glass (6 mm thickness) or deionized water was used as the confinement layer medium. All the experiments were repeated three times and average values were used.

Talyscan surface profiler was used to measure the depth and diameter of the deformed craters. Scanning electron microscopy and optical microscopy were used to visualize the surfaces of the craters in copper foil and aluminum foil ablative overlay. A photodetector and an oscilloscope were used to determine the time profile of the laser pulse.

2.2. Plasma visualization and characterization

Photron FASTCAM SA5 high-speed camera was used to capture the formed plasma in this study. The camera has a maximum exposure time of 1 μs and a wide range of frame rates [50 to 150000 fps (frames/sec)], out of which 5000 fps was mainly used in order to capture the entire plasma image. In addition, the plasma images were captured at the maximum frame rate (150000 fps) of the camera to understand the evolution of plasma. The camera was positioned at an angle of β (35°) to the path of the laser beam as illustrated in Fig. 2a. The entire evolution of laser-induced plasma from its formation to the vanishing was recorded for the analysis.

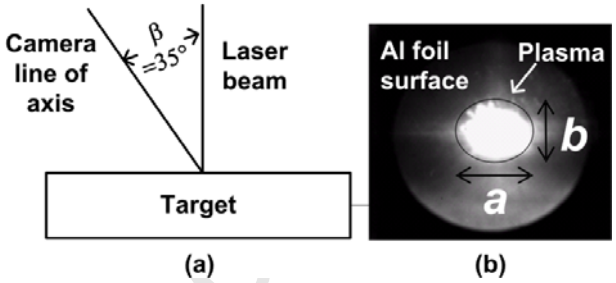

Fig. 2. Measurement method for the plasma diameter (a) Orientation of camera with the laser beam (b) Image of plasma acquired by high speed camera

The shape and size of the plasma change with the observation angle (β) of the camera. Therefore, change factor of plasma size was used instead of the absolute plasma sizes in this analysis. The plasma images were acquired at regular time intervals (200 μs) by the high speed camera from which the plasma diameter and its change factor were estimated. The plasma was seen as a bright spot in the acquired image as shown in Fig. 2b. The area of actual illumination ($A=\pi ab$) was calculated

from the minor and major axes lengths as the plasma shape is observed to be approximately elliptical. As the camera line of axis is 35° (β) inclined to the laser beam axis, the actual illumination area (A) has to be projected to a plane perpendicular to the camera axis to calculate the projected illumination area ($A_p = A \cos\beta$) . From A_p, the projected illumination diameter ($D=\sqrt{(4 * A_p/\pi)}$) was calculated, assuming that the projected shape of the plasma is circular. From this projected diameter (D), the plasma diameter (D_P) was calculated by making a comparison with the initial projected diameter (D_0) corresponding to the laser beam spot size of 0.6 mm ($D_P = 0.6*D/D_0$). The change in plasma size at different time periods with respect to initial plasma size was characterized by the change factor (D/D_0).

3. Results and discussions

3.1. Evolution of laser-induced plasma

The evolution of plasma upon single pulse ablation and a continuous ablation of 45 laser pulses at a frequency of 6 KHz was analyzed for the laser fluence of 7.3 J/cm^2. Water with 4 mm thickness was used as the confinement layer.

Fig. 3. Evolution of plasma for single pulse ablation at 7.3 J/cm^2 laser fluence (Camera frame rate = 150000 fps)

The evolution of plasma for single laser pulse ablation was analyzed using the plasma images acquired at the frame rate of 150000 fps. Fig. 3 shows the sequence of plasma images with respect to time. It can be observed that the plasma was visible at 6.67 µs whereas it disappeared at 13.3 µs. Since there is a possibility of plasma formation instantly after the firing of laser pulse and the plasma disappearance anytime before 13.3 µs, the plasma lifetime, starting from plasma formation, expansion, decaying to vanishing for single pulse ablation is approximated to be less than 13.3 µs. In comparison with the literature, Tanski et al. [14] observed a total plasma lifetime of 80 ns in their experiment which was slightly more than the laser pulse duration of 55 ns; the plasma expansion occurred until 22 ns (after the laser peak position) and then the plasma started decaying. However, in an

experiment by Barthelemy et al. [17], for a 10 ns pulse width using XeCl excimer laser pulse irradiation on aluminum target, the plasma lifetime lasted longer than 500 ns, i.e. 50 times the pulse duration. In that case, the significant plasma expansion occurred during the first 10 ns to 100 ns, after which the plasma decayed [17]. In our experiments, the exact plasma lifetime and the plasma evolution phases starting from plasma formation, expansion, decay to vanishing upon a laser pulse have been difficult to observe due to the larger time interval of 6.67 μs between two frames compared to the laser pulse duration of 38 ns.

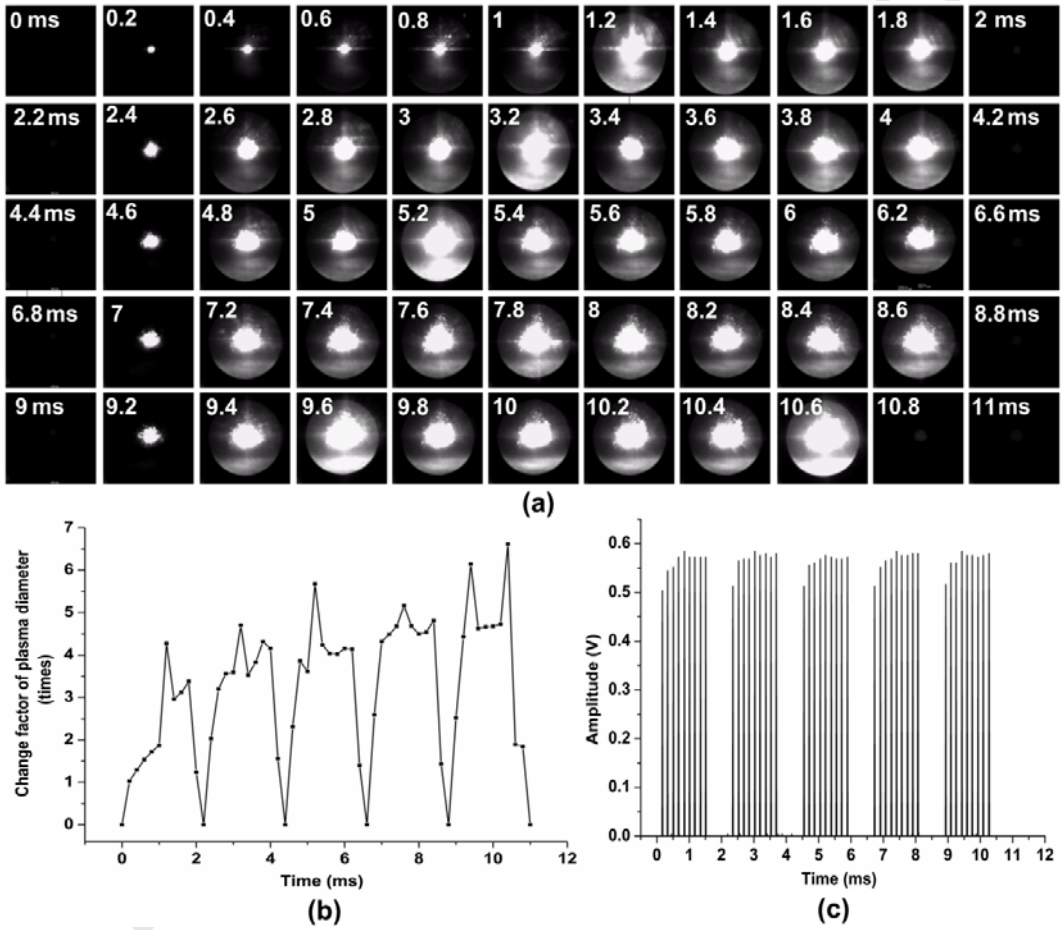

Fig. 4. Evolution of plasma for ablation of 45 pulses at 7.3 J/cm^2 laser fluence (a) Sequence of plasma images captured at regular time intervals by high speed camera (b) Change factor of plasma diameter with respect to time (c) Voltage amplitude of laser pulses measured using photodetector

The analysis of plasma evolution for the ablation of 45 laser pulses is shown in Fig. 4. In this analysis, 45 pulses were applied through 5 cycles with 9 pulses in each cycle, which can be witnessed from Fig. 4c that illustrates the time profile of laser

pulses measured by the photodetector. Fig. 4a shows the sequence of plasma images taken at regular time intervals by the high speed camera with a frame rate of 5000 fps. The change in plasma size with time is illustrated in Fig. 4b. It is revealed from the plasma images that, in each cycle, the plasma was smaller at the first pulse, which then increased gradually and reached the maximum size during the fifth or sixth laser pulse. After attaining the maximum, the plasma decreased in size during the subsequent pulses. In continuous ablation of 45 pulses with the frequency of 6000 Hz, the plasma lifetime for one laser pulse of 13.3 μs was 12.5 times shorter than the pulse repetition time of 166.67 μs. Thus, there was no interference of plasma evolution from subsequent laser pulses as the plasma formed with each pulse completely vanished before the next laser pulse. The plasma behavior was similar when the glass confinement or direct ablation conditions were used.

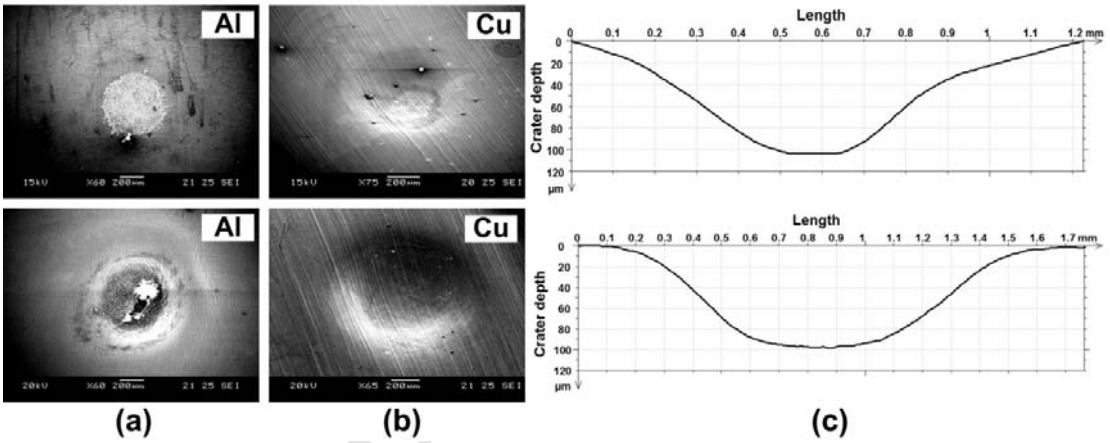

Fig. 5. Comparison of crater formation on copper foil between single pulse (top) and 45 pulses (bottom) ablation at 13.6 J/cm^2 laser fluence: (a) SEM image of aluminum foil top surface (b) SEM image of the crater top surface on copper foil (c) Cross-sectional profile of the crater at its center

The crater formation on copper foil was compared between single pulse and 45 pulses. Fig. 5 compares the top surfaces of the aluminum foil ablative overlay and the crater on copper foil between one pulse and 45 pulses. It is observed that single pulse ablation was sufficient to produce a crater. When the number of pulses was increased to 45, the crater diameter increased by about 25% to that of one pulse as shown in Figs. 5b and 5c. Correspondingly, the vaporization area in aluminum foil after 45 pulses was larger than that of one pulse as shown in Fig. 5a. The vaporization depth and area of aluminum foil increased with the increase in laser

pulses, which hence increased the size of the plasma as seen in Fig. 4a. Therefore, it can be understood that the increase in crater diameter is in correlation with the plasma propagation in the radial direction.

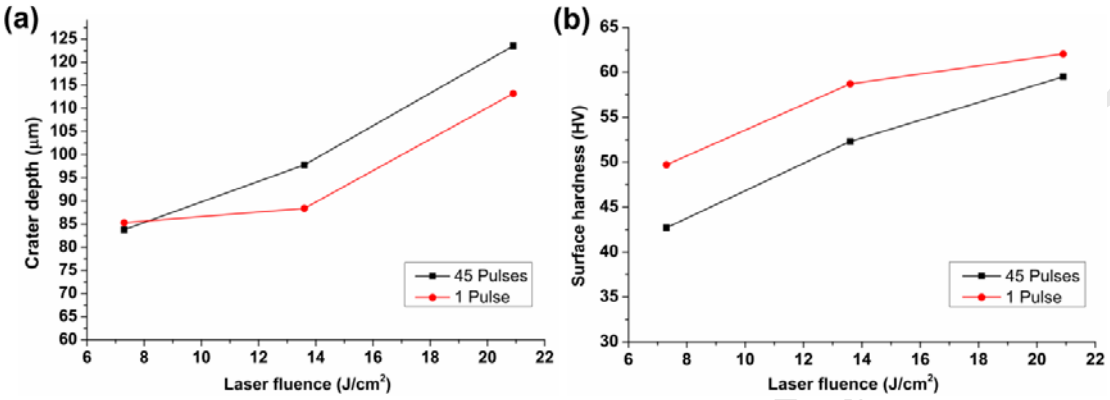

Fig. 6. Comparison of deformation craters between one pulse and 45 laser pulses (a) Crater depth (b) Crater top surface hardness

The comparison of deformation depth and top surface hardness of the craters between one pulse and 45 pulses for various laser fluences is illustrated in Fig.6. It is revealed from Fig. 6a that more than 90% of the final depth of the formed crater was achieved during the first pulse itself. During the subsequent laser pulses, only 10% increase in crater depth was observed. This behavior can be attributed to one or more of the following effects:

(a) Once the deformation of copper foil is started upon the first pulse, the yield stress of material increases due to the workhardening behavior. This effect is evident from Fig. 6b where the hardness of the top crater surface after the first pulse is higher than the hardness after multiple pulses. The reduction in hardness with the multiple pulses could be due to the direct heating of copper surface as the overlay aluminum foil is completely vaporized. Due to the workhardening of foils after the first pulse, further plastic deformation during the subsequent pulses is restricted and only a small increase in crater depth was observed with the increase in number of pulses.

(b) During the deformation of copper foil with the first pulse, the aluminum foil overlay moves along with the copper foil as both the foils are firmly sealed together using the vacuum grease. This movement of aluminum foil provides a defocussing effect during subsequent pulses and reduces the laser intensity on the Al foil surface. This

would have caused lesser vaporization and hence smaller increase in crater depth after the first pulse.

(c) As seen in Fig. 4a, the plasma is confined to a smaller area during the first pulse compared to the latter pulses for similar laser intensities. The increase in plasma size during multiple pulses leads to the reduction in plasma density and shock pressure and hence the plastic deformation of foil.

It is evident from Fig. 4 that the plasma propagation occurred along the irradiated surface of the aluminum foil. It is also observed that the radial propagation of plasma along the surface was approximately circular even though the laser beam was square-shaped. This behavior is consistent with the literature in which the shape of the laser-irradiated plasma plume and the shockwave were observed to be hemi-spherical while expanding both in ambient air [14, 17] and in water [18]. The propagation in axial direction has been restricted by water confinement in one direction and metal foil in the other direction.

This study further focused on the extent of plasma expansion (maximum plasma size) to analyze the correlation between the plasma propagation and the metal foil deformation.

3.2. Effect of laser fluence

The evolution of plasma for 45 pulses ablation at three different laser fluence values was tested. Water with 4 mm thickness was used as the confinement layer.

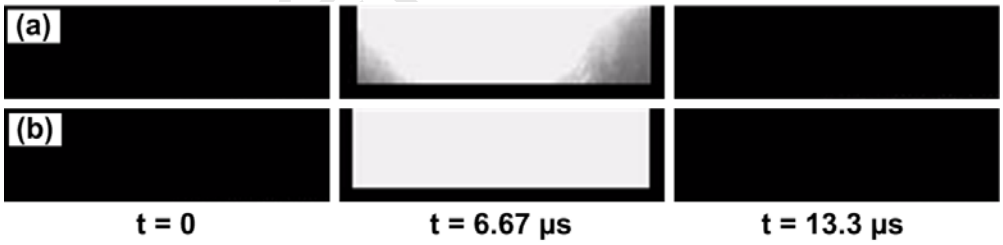

Fig.7. Comparison of plasma evolution at different laser fluence (a) 7.3 J/cm^2 (b) 13.6 J/cm^2

Fig. 7 compares the plasma evolution for single pulse ablation for different laser fluences. It can be observed that the lifetime of plasma for single laser pulse (lesser than 13.3 µs) remained the same irrespective of the laser fluence. Fig. 8 compares the plasma image at different laser fluences for the time duration of 9.4 ms. It can be

identified from Fig. 8 that the plasma behavior varied significantly at 20.9 J/cm^2 fluence. At lower fluences (7.3 J/cm^2 and 13.6 J/cm^2), radial plasma propagation occurred along the interface between the water and aluminum foil. Whereas, at higher fluence (20.9 J/cm^2), the plasma was seen both at the water-air interface and the water-aluminum foil interface. This observation confirms the occurrence of dielectric breakdown at the water-air interface at higher intensities [12]. The dielectric breakdown phenomenon occurs due to one or more of the following mechanisms: cascade ionization, multiphoton ionization, and the surface impurities [19, 20].

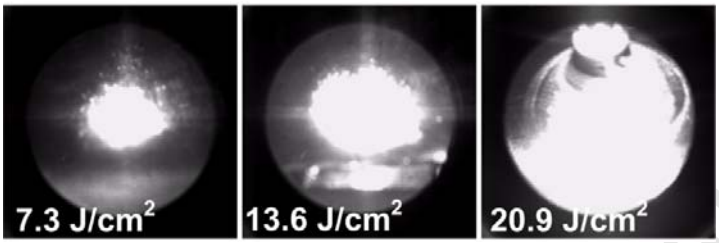

Fig. 8. Effect of laser fluence on the evolution of laser-induced at 9.4 ms

The correlation between the change factors of crater size and plasma size with increase in laser fluence is illustrated in Fig. 9. The peak laser-induced shock pressure was calculated using Fabbro's model and plotted in Fig. 9b. The peak shock pressure according to Fabbro's model is given as [21]:

$$P\ (GPa) = 0.01\sqrt{\frac{\alpha}{3+2\alpha}}\sqrt{I_0\left(\frac{GW}{cm^2}\right)\ Z\left(\frac{g}{cm^2 s}\right)} \quad (1)$$

where I_0 is the laser intensity, α is the fraction of internal energy used in increasing the thermal energy of plasma which is assumed to be 0.1. Z is the shock impedance given as, $Z = 2/(1/Z_1 + 1/Z_2)$ where Z_1 and Z_2 are the shock impedances of target material and confinement medium. The shock impedances of aluminum foil target and water confinement are 1.5 x 10^6 g/cm^{2}s and 0.165 x 10^6 g/cm^{2}s, respectively.

When the laser fluence was increased by the order of 2.86 times from 7.3 J/cm^2 to 20.9 J/cm^2, the maximum plasma diameter increased accordingly by the order of 2.18 times (Fig. 9b). Consecutively, it is observed that the change factor of maximum shock pressure (1.69 times) was smaller than that of plasma diameter. The change factor of crater depth was 1.47 times, which correlates well with that of maximum

shock pressure. Interestingly, it can be noted from Fig.9 that the change factor has been descending in the order of laser fluence (2.86), maximum plasma diameter (2.18), maximum shock pressure (1.69), and crater depth (1.47). With increase in laser fluence, the shock pressure, i.e. the forming load increased, resulted in increased plastic deformation of foils and thus deeper craters. Meanwhile, the crater diameter increased only by a small amount in the order of 1.13 times (Fig. 9b) as the crater diameter is influenced mainly by the laser beam size which has been constant throughout the analysis.

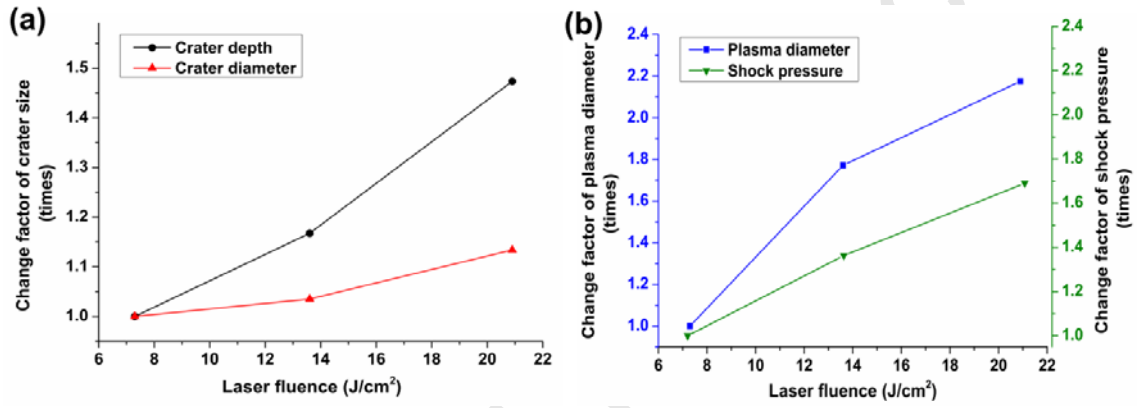

Fig.9. Comparison of change factor of crater size with the change factor of maximum plasma diameter and theoretical shock pressure at different laser fluences

It can be observed from Fig. 9b that both the plasma diameter and pressure increased simultaneously with increase in laser fluence. It is interesting to observe that, even though the plasma propagated to a larger distance of about 7 mm, the crater diameter (1 mm) was not increased significantly. As the distance from the center of irradiation increased, the plasma density decreased correspondingly. Therefore, at foil positions distant from the irradiation spot, the plasma density was less and hence the resultant shock pressure was insufficient to induce the plastic deformation.

The measured plasma diameter at 20.9 J/cm^2 was slightly larger than the actual diameter. This could be due to the scattering of light by the shockwave propagating at the top surface (as shown in Fig. 8).

3.3. Effect of confinement medium

The influence of confinement layer materials such as fused silica glass and deionized water on the plasma evolution has been analyzed at laser ablation of 45

pulses. The major difference observed between the glass and water confinement mediums is the occurrence of dielectric breakdown phenomenon at higher laser fluence. Fig. 10 compares the images of plasma at 20.9 J/cm^2 laser fluence with water and glass confinement layers. Plasma observation at the water top surface in Fig. 10a indicates that the dielectric breakdown of water occurred at the interface between the air and water top surface. Whereas, with the glass confinement, dielectric breakdown occurred at the interface between the bottom surface of glass and the ablative overlay as shown in Fig. 10b. The damage of glass can be attributed to the reflectivity of the target and the collision of metal plasma with the rear surface of the glass [19].

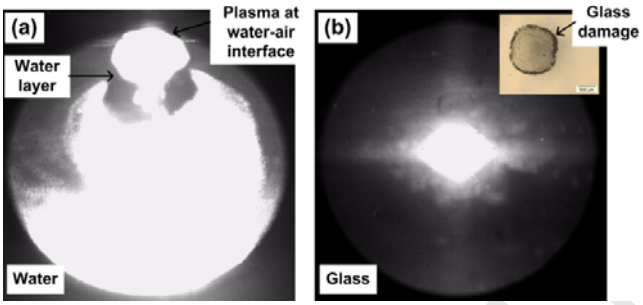

Fig. 10. Comparison of dielectric breakdown mechanism between water and glass confinements at 20.9 J/cm^2 laser fluence (a) Water confinement (b) Glass confinement

Fig. 11 illustrates the correlation between the change factor of crater size and the change factor of maximum plasma diameter for water and glass confinements. For 2.86 times increase in laser fluence, the plasma diameter increased by the order of 3.28 times in glass whereas it increased only by 2.18 times in water. Correspondingly, the change factor of crater depth was higher in glass (2.57 times) than in water (1.47 times) as shown in Fig. 11a. The increase in crater diameter too was higher with glass (1.44 times) than with water (1.13 times). Furthermore, the actual crater depth and diameter were higher with glass. This higher crater size in glass was observed to be mainly influenced by the propagation characteristics of plasma. It is found from the results that the expansion of plasma is more restrictive in glass, causing smaller plasma diameter. Therefore, in glass, the plasma was confined to a narrow region resulting in higher density of plasma. The denser plasma caused higher shock pressure (forming load) and hence deeper craters were produced with the glass confinement. Meanwhile, as the plasma expansion

proceeded to a larger distance in water, the plasma density and pressure were reduced. The diameter of plasma during the first pulse was approximately constant between water and glass confinements. The maximum plasma diameter occurred for the time period ranging between 7 ms to 10.6 ms.

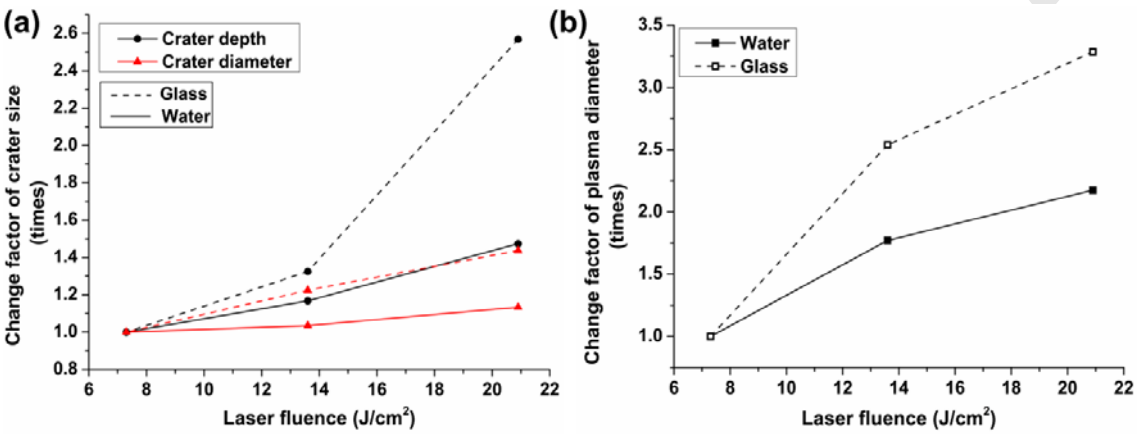

Fig.11. Comparison of the change factor of crater size and the change factor of maximum plasma diameter between water and glass confinement layers

The larger actual size and change factor of craters in glass confinement can also be attributed to the following behaviors: (i) As the transmittivity of fused silica glass (94%) is higher than that of water (81%), incident laser energy on ablative overlay is higher with glass. (ii) Dielectric breakdown of water at its top surface tends to reduce the incident laser energy (iii) During FPLSF with water confinement, only a small thickness of ablative overlay (aluminum foil) was ablated as shown in Fig. 5a until the laser fluence reached 20.9 J/cm^2. Therfore, the shockwave propagating from the top surface of aluminum foil experienced attenuation at the remaining aluminum foil thickness before reaching the copper foil. This shockwave attenuation resulted in the reduction of shock pressure. With glass confinement, the entire thickness of the aluminum foil was ablated even at the lower fluences due to the higher transmittivity of fused silica glass. Therefore, the copper foil top surface was directly exposed to the laser beam and experienced ablation at its top surface upon irradiation. The ablation depth and area of copper foil increased with the increase in fluence causing a reduction in foil thickness. The reduction in thickness resulted in the increase in material velocity and the deformation depth. Furthermore, as there was no shockwave attenuation with glass confinement as in water confinement, the shock pressure was higher with glass. These two behaviors, reduction in copper foil

thickness and increase in shock pressure together caused larger increase in crater depth and diameter with glass confinement than with water. (iv) Shockwave structures were formed on copper foils with glass confinement due to the direct irradiation of copper foil top surface. As a result of shockwave formation, the increase in crater diameter was higher with glass whereas only uniform hemispherical craters were formed with water confinement.

3.4. Effect of confinement thickness

The effect of confinement layer (water) thickness on the plasma propagation was analyzed at the following thickness levels: 4 mm, 6 mm, and 7 mm. Two laser fluence levels, 7.3 J/cm^2 and 13.6 J/cm^2 and 45 laser pulses were used. A correlation between the change factors of crater size and plasma size for different confinement thicknesses is shown in Fig 12. With constant laser fluence, a reduction in plasma diameter was observed when the confinement thickness was increased from 4 mm to 7 mm (Fig. 12b). This behavior can be attributed to the absorption of laser energy within the confinement thickness.

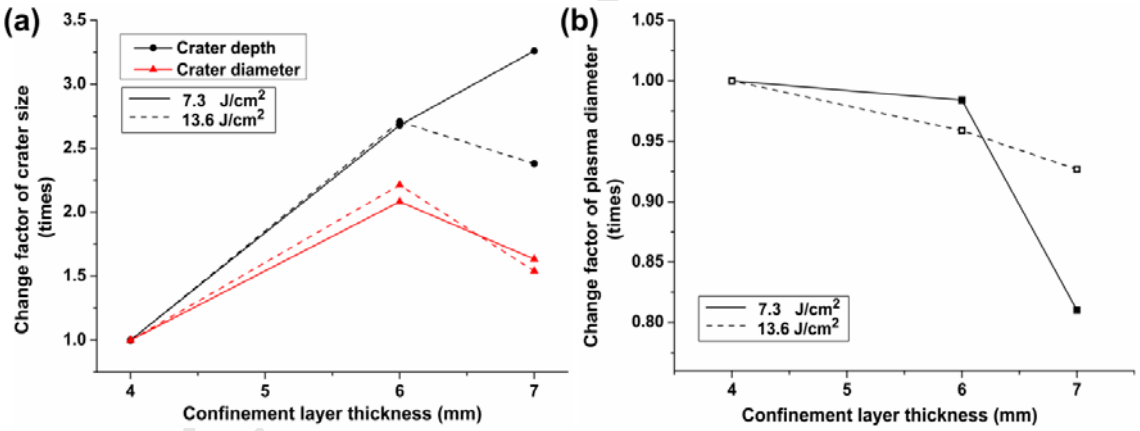

Fig.12. Correlation between change factors of crater size and plasma size at different confinement layer thicknesses

It can be observed from Fig. 12a that both the crater depth and diameter increased with the increase in confinement thickness from 4 mm to 6 mm at both 7.3 J/cm^2 and 13.6 J/cm^2 fluences. As the laser energy experiences absorption within the confinement, reduction in crater size was expected with increase in confinement thickness. As mentioned earlier, Morales et al. [3] observed the influence of confinement thickness on plasma pressure as the arrival of shockwave before the occurrence of laser peak reduces the plasma pressure. For the confinement

thickness (t) of 4 mm in FPLSF, the time (τ) taken by the shockwave to reach the water-air interface is calculated to be 2.4 μs considering the shock velocity (D) in water as 1650 ms^{-1}. As this time is much longer than the pulse duration of 38 ns, this behavior could not be the reason for lesser shock pressure and crater depth at smaller confinement thickness. Ocana et al. [4] found numerically that the plasma pressure increases with increase in confinement thickness. In this study, reduction in plasma diameter was observed with the increase in confinement thickness (Fig. 12b). The correlation between plasma diameter and plasma pressure with increase in confinement thickness confirms that the reduction in plasma diameter increases the plasma density and pressure due to the confinement of plasma. Hence, the increase in crater depth and diameter is attributed to the reduction in plasma diameter with increase in confinement thickness.

However, the crater depth at 13.6 J/cm^2 and crater diameter at both fluences decreased at the confinement thickness of 7 mm (Fig. 12a). The possibility of dielectric breakdown at higher confinement thickness was suggested by Ocana et al. [4]. However, there was no dielectric breakdown of water observed at 7 mm in our experiment. Therefore, the reduction in plastic deformation could be due to large absorption of laser energy by the confinement thickness. The results highlight that there exists an optimum thickness of confinement layer to achieve larger plasma pressure and the plastic deformation.

4. Conclusions

This paper experimentally analyzed the influence of plasma evolution on the plastic deformation of metal foils in flexible pad laser shock forming using a high-speed camera. Some important findings of this study are as follows:

- The plasma lifetime, starting from plasma formation, expansion, decay to vanishing for single pulse ablation was less than 13.3 μs irrespective of the confinement conditions.
- For 45 pulses ablation as 5 cycles with 9 pulse train in each cycle, the plasma size increased gradually and attained maximum at fifth or sixth cycle. The plasma evolution from each pulse did not interfere with each other.
- The single pulse ablation was sufficient to produce craters whereas the crater depth and diameter were smaller by 10% and 25% respectively compared to that of 45 pulses.
- The laser fluence is found to have significant influence on the plasma evolution in water confinement. For laser ablation of 45 pulses, when the laser fluence was increased by 2.86 times, the change factors of maximum plasma diameter (2.18), maximum shock pressure (1.69), and crater depth (1.47) decreased in the same order.
- A significant difference in plasma evolution characteristics was observed between water and glass confinement layers. At higher laser fluence, dielectric breakdown occurred at the water-air interface with water whereas it occurred at the glass-ablative layer interface with glass. The confined plasma in glass increased the plasma density and pressure resulting in deeper craters.
- When the water confinement thickness was increased, increase in crater size was observed in spite of the laser energy absorption within the confinement. Though this behavior was attributed to the corresponding reduction in plasma size, a detailed analysis is required to understand the correlation between plasma evolution and confinement layer thickness.

Acknowledgement

This work is supported by Machining Technology Group, Singapore Institute of Manufacturing Technology under CRP Project Number U11-M-013U and Nanyang Technological University research scholarship.

References

[1] B. Nagarajan, S. Castagne, Z. Wang, Mold-free fabrication of 3D microfeatures using laser-induced shock pressure, Appl. Surf. Sci., 268 (2013) 529-534.

[2] B. Nagarajan, S. Castagne, Z. Wang, Influence of Process Parameters on the Deformation of Copper Foils in Flexible-Pad Laser Shock Forming, in: 8th International Conference on MicroManufacturing, University of Victoria, Victoria, BC, Canada, 2013.

[3] M. Morales, J.A. Porro, M. Blasco, C. Molpeceres, J.L. Ocaña, Numerical simulation of plasma dynamics in laser shock processing experiments, Appl. Surf. Sci., 255 (2009) 5181-5185.

[4] J.L. Ocana, M. Morales, C. Molpeceres, J.A. Porro, Laser Shock Processing of Metallic Materials: Coupling of Laser-Plasma Interaction and Material Behaviour Models for the Assessment of Key Process Issues, AIP Conference Proceedings, 1278 (2010) 902-913.

[5] A. Gupta, B. Braren, K.G. Casey, B.W. Hussey, R. Kelly, Direct imaging of the fragments produced during excimer laser ablation of $YBa_2Cu_3O_{7-\delta}$, Appl. Phys. Lett., 59 (1991) 1302-1304.

[6] R.M. Gilgenbach, P.L.G. Ventzek, Dynamics of excimer laser-ablated aluminum neutral atom plume measured by dye laser resonance absorption photography, Appl. Phys. Lett., 58 (1991) 1597-1599.

[7] H. Nose, H. Maeda, M. Nakahara, Observation and application of laser induced shock wave, in: 18th International Conference on Advanced Information Networking and Applications, 2004, pp. 215-218.

[8] K. Watanabe, H. Torikai, Q.S. Yang, A. Sasoh, Y. Sano, N. Mukai, Shock wave phenomena in underwater laser peening, in: Z. Jiang (Ed.) Shock Waves, Springer Berlin Heidelberg, 2005, pp. 1039-1042.

[9] H. Hirahara, M. Fujinami, M. Kawahashi, Optical Measurement of a Laser Induced Micro Shock Wave on a Metal Surface, Journal of Fluid Science and Technology, 3 (2008) 965-974.
[10] J. Noack, D.X. Hammer, G.D. Noojin, B.A. Rockwell, A. Vogel, Influence of pulse duration on mechanical effects after laser-induced breakdown in water, J. Appl. Phys., 83 (1998) 7488-7495.
[11] N. Seto, High-speed simultaneous observation of plasma and keyhole behavior during high power CO_2 laser welding: Effect of shielding gas on porosity formation, J. Laser Appl., 12 (2000) 245-250.
[12] L. Berthe, R. Fabbro, P. Peyre, L. Tollier, E. Bartnicki, Shock waves from a water-confined laser-generated plasma, J. Appl. Phys., 82 (1997) 2826-2832.
[13] S. Amoruso, R. Bruzzese, N. Spinelli, R. Velotta, Characterization of laser-ablation plasmas, J. Phys. B-At. Mol. Opt. Phys., 32 (1999) R131.
[14] M. Tanski, M. Kocik, R. Barbucha, K. Garasz, J. Mizeraczyk, Time-Resolved Observation of the Ablation Plasma Plume Dynamics during Nanosecond Laser Micromachining, in: Symposium on Photonics and Optoelectronics (SOPO), 2012, pp. 1-4.
[15] F. Docchio, P. Regondi, M.R.C. Capon, J. Mellerio, Study of the temporal and spatial dynamics of plasmas induced in liquids by nanosecond Nd:YAG laser pulses. 1: Analysis of the plasma starting times, Appl. Optics, 27 (1988) 3661-3668.
[16] M. Cirisan, J.M. Jouvard, L. Lavisse, L. Hallo, R. Oltra, Laser plasma plume structure and dynamics in the ambient air: The early stage of expansion, J. Appl. Phys., 109 (2011) 103301.
[17] O. Barthelemy, J. Margot, M. Chaker, Characterization of the expansion of an aluminum laser-induced plasma in ambient air by fast photography, IEEE Transactions on Plasma Science, 33 (2005) 476-477.
[18] L. Martí-López, R. Ocaña, J.A. Porro, M. Morales, J.L. Ocaña, Optical observation of shock waves and cavitation bubbles in high intensity laser-induced shock processes, Appl. Optics, 48 (2009) 3671-3680.
[19] D. Devaux, R. Fabbro, L. Tollier, E. Bartnicki, Generation of shock waves by laser-induced plasma in confined geometry, J. Appl. Phys., 74 (1993) 2268-2273.
[20] N.B. Dahotre, S.P. Harimkar, Laser Fabrication and Machining of Materials, in, Boston, MA : Springer Science + Business Media, LLC., 2008.

[21] R. Fabbro, J. Fournier, P. Ballard, D. Devaux, J. Virmont, Physical study of laser-produced plasma in confined geometry, J. Appl. Phys., 68 (1990) 775-784.

Figure Captions

Figure 1. Schematic of flexible pad laser shock forming with high speed camera for plasma visualization

Figure 2. Measurement method for the plasma diameter (a) Orientation of camera with the laser beam (b) Image of plasma acquired by high speed camera

Figure 3. Evolution of plasma for single pulse ablation at 7.3 J/cm^2 laser fluence (Camera frame rate = 150000 fps)

Figure 4. Evolution of plasma for ablation of 45 pulses at 7.3 J/cm^2 laser fluence (a) Sequence of plasma images captured at regular time intervals by high speed camera (b) Change factor of plasma diameter with respect to time (c) Voltage amplitude of laser pulses measured using photodetector

Figure 5. Comparison of crater formation on copper foil between single pulse (top) and 45 pulses (bottom) ablation at 13.6 J/cm^2 laser fluence: (a) SEM image of aluminum foil top surface (b) SEM image of the crater top surface on copper foil (c) Cross-sectional profile of the crater at its center

Figure 6. Comparison of deformation craters between one pulse and 45 laser pulses (a) Crater depth (b) Crater top surface hardness

Figure 7. Comparison of plasma evolution at different laser fluence (a) 7.3 J/cm^2 (b) 13.6 J/cm^2

Figure 8. Effect of laser fluence on the evolution of laser-induced at 9.4 ms

Figure 9. Comparison of change factor of crater size with the change factor of maximum plasma diameter and theoretical shock pressure at different laser fluences

Figure 10. Comparison of dielectric breakdown mechanism between water and glass confinements at 20.9 J/cm^2 laser fluence (a) Water confinement (b) Glass confinement

Figure 11. Comparison of the change factor of crater size and the change factor of maximum plasma diameter between water and glass confinement layers

Figure 12. Correlation between change factors of crater size and plasma size at different confinement layer thicknesses